Available online at www.sciencedirect.com
ScienceDirect
Sensors and Actuators A 138 (2007) 230–238
SENSORS AND ACTUATORS A PHYSICAL
www.elsevier.com/locate/sna

Design and development of a 331-segment tip–tilt–piston mirror array for space-based adaptive optics

Jason B. Stewart [a,*], Thomas G. Bifano [b,c], Steven Cornelissen [c], Paul Bierden [c], B. Martin Levine [d], Timothy Cook [e]

[a] *Department of Electrical and Computer Engineering, Boston University, Boston, MA, United States*
[b] *Department of Manufacturing Engineering, Boston University, Boston, MA, United States*
[c] *Boston Micromachines Corporation, Watertown, MA, United States*
[d] *Jet Propulsion Laboratory, California Institute of Technology, Pasadena, CA, United States*
[e] *Department of Astronomy, Boston University, Boston, MA, United States*

Received 31 August 2006; received in revised form 12 April 2007; accepted 20 April 2007
Available online 4 May 2007

Abstract

We report on the development of a micromachined silicon deformable mirror (DM) system for the hyper-contrast visible nulling coronagraph architecture designed by the Jet Propulsion Laboratory for NASA's Terrestrial Planet Finding (TPF) mission. The new DM is designed to achieve unprecedented optical quality and mechanical positioning precision as required by the nulling coronagraph. It consists of 331 close-packed hexagonal segments on a 600 μm pitch. Each segment has three adjustable degrees of freedom controlling out-of-plane rotation (in two axes) and surface normal motion over a continuous range of ±3 mrad and 1 μm, respectively. The coronagraph implementation specifies that each segment maintains an overall flatness better than 10 nm RMS, irrespective of segment angle. To achieve this objective, two design concepts were developed in parallel. The first design uses thick mirror segments consisting of epitaxial grown polysilicon (epipoly) to provide the mirror with high rigidity, allowing it to tilt without bending. The epipoly layer can also be highly polished to better than 1nm RMS local surface roughness. The second design uses thinner, more compliant mirror segments, but supports them with flexure-based electrostatic actuators that decouple tilt motion from mirror segment bending moments. The thinner mirror segment has reduced optical quality due to print-through effects, but offers greater ease in post-processing mirror curvature caused by residual stress gradients. DM segments fabricated with the flexure design experience a maximum mirror bend of 2.8 nm RMS at 4.3 mrad of tilt. Both DM designs and associated microfabrication processes are presented. Optical and electromechanical characterization results are also presented.

Keywords: MEMS; Deformable mirror; Adaptive optics; Amplitude correction; Phase correction; Coronagraph

1. Introduction

The NASA TPF mission seeks to optically detect, characterize and study Earth-like extrasolar planets located in the habitable zones of nearby stars. In an effort to determine if these planets are capable of harboring life, the light reflected and emitted from these planets will be captured and examined by two observatories based in space, one operating in the infrared and the other in the visible. In order to improve the contrast ratio of light detected from the planet, both observatories are faced with the non-trivial challenge of suppressing starlight emitted from the parent star [1].

The DM presented here was developed for a space-based visible nulling coronagraph instrument. The nulling coronagraph is a Mach-Zehnder style shearing interferometer coupled with a coherent fiber optic spatial filter array that can be used behind a single aperture telescope to enhance the contrast ratio of planet images to the level necessary for detection. A candidate star that is located on the telescope axis is destructively interfered by the nuller, while planet light that is off-axis passes through the coronagraph optics for detection. For successful planet imaging, parent starlight must be suppressed by a factor of 10^{-10}, which is determined by the observation spectrum and planet size. To

* Corresponding author at: 8 Saint Mary's St, Boston, MA 02215, United States. Tel.: +1 617 353 9961.
E-mail address: jstew@bu.edu (J.B. Stewart).

0924-4247/$ – see front matter © 2007 Elsevier B.V. All rights reserved.
doi:10.1016/j.sna.2007.04.051

achieve this contrast ratio, the nulling coronagraph optical system employs a DM that can control local wavefront phase and amplitude. Phase is adjusted by moving mirror segments in a surface normal direction. Amplitude is adjusted by tilting the segment, coupling more or less of the subaperture light into its corresponding spatial filter optical fiber. The success of the interferometer and spatial filter combination to produce nulls to the level necessary for planet detection strongly depends on DM performance [2,3].

Wavefront aberrations in space-based stellar observatories are slowly varying, and created by imperfect optics, shifts in telescope alignment during launch, and thermal fluctuations during observation. For the nulling coronagraph it is essential to have high precision positioning resolution, nanometer level stability, and hysteresis-free motion, all of which are achievable with an electrostatically controlled MEMS DM. For successful implementation into the nulling coronagraph, each mirror segment in the new DM must have a positioning resolution of 0.1nm in the surface normal direction (i.e. "piston") and 0.3 μrad in out of plane rotation (i.e. "tilt"), without hysteresis. Previously developed segmented BU DM technology, which provided the foundation for this new design, has demonstrated nanometer-level repeatability and is absent of hysteresis.

To meet coronagraph optical specifications, each DM segment must have a surface flatness of less than 10 nm RMS. This is both a static and dynamic requirement for the DM segments. The design, fabrication and control of mirror segments with this flatness requirement are significant challenges and the focus of this work [4]. The difficulties in achieving this specification are due to the tendency of thin MEMS polysilicon components to bend during actuation and curl when released due to residual stress gradients embedded in the deposited material. Two device architectures that are capable of achieving this flatness requirement, as well as their optical and electromechanical performance, are presented. A detailed comparison of both designs is given and plans for future mirror development are discussed.

2. The device

2.1. Architecture

The new nulling coronagraph DM architecture (referred to hereafter as the TPF DM) is based largely upon existing MEMS DM technology at Boston University, tailored to the requirements of the visible nulling coronagraph. Existing DMs are fabricated at a MEMS foundry using a wafer-scale three-layer polycrystalline silicon (polysilicon) surface micromachining process that uses phosphosilicate glass (PSG) as a sacrificial material. DMs are also diced and released at the foundry. Mirrors are deformed using surface-normal electrostatic actuators. The actuators are comprised of a compliant electrode diaphragm (second polysilicon layer) supported along two edges above a fixed electrode (first polysilicon layer). The top surface of the actuator diaphragm is connected to the mirror surface (third polysilicon layer) by an anchoring post at its center. The mirror reflectivity is enhanced with a gold coating deposited on the final polysilicon layer [5,6].

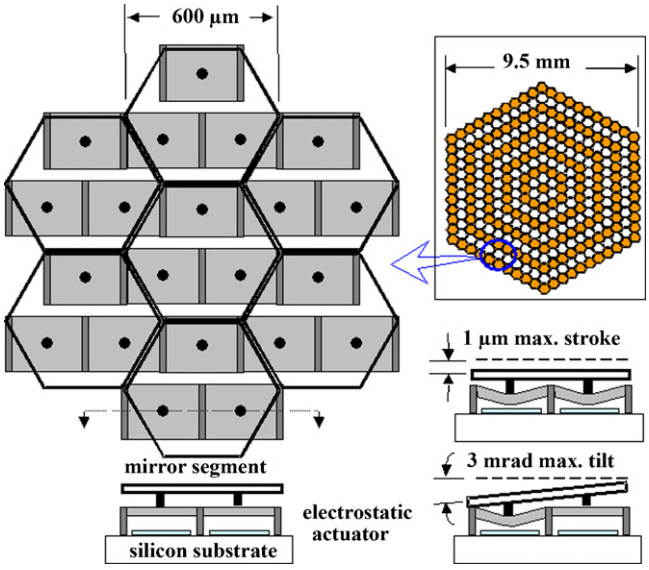

Fig. 1. Top and side view of the new MEMS TPF DM architecture for tip/tilt and piston motion.

A schematic and summary for the TPF DM design can be seen in Fig. 1. The DM consists of 331 hexagonal mirror segments, each supported by three independent electrostatic actuators. The three actuators are connected to the hexagonal mirror segment via posts and provide the mirror with three degrees of freedom—tip, tilt and piston. The mirror actuators can simultaneously provide the mirror with the 1 μm of stroke and 3 mrad of tilt required for the nulling coronagraph. The mirror segments span 600 μm and create a total DM aperture diameter of 9.5 mm.

2.2. Fabrication process

Fabrication of the TPF DM begins with a three-layer polysilicon surface micromachining process (similar to the inherited process) that involves the deposition and patterning of alternating layers of sacrificial and structural thin films (Fig. 2). The first and second polysilicon layers in the developed process are 500 nm and 2 μm thick, respectively, and the two sacrificial oxide layers are 5 μm thick. The third polycrystalline silicon layer is 3 μm thick and can be used as a seed layer for a thicker epitaxial grown polysilicon layer or as the final mirror segment surface (pre-metal deposition) depending on the mirror segment design, which is discussed in more detail below.

The remaining mirror fabrication steps consist of the deep reactive ion etch (DRIE) of the final or top polysilicon layer(s) to partition the 331 hexagonal mirror segments (stopping in the second oxide layer), a hydrofluoric acid wet etch of the sacrificial oxide layers to release the micromirror array and a CO_2 supercritical dry. The mirror surface is then coated with a 100 nm layer of evaporated gold to enable broadband reflectance in the visible to near infrared. To reduce the diffraction of reflected light, no oxide etch-access holes are used in the mirror surface. A polishing step is used after the second oxide deposition to further reduce print-through of the underlying layers to the mirror segment layer.

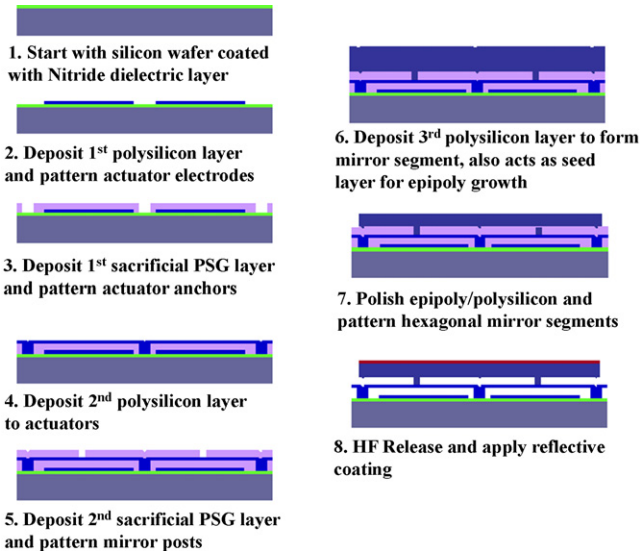

Fig. 2. Profile of microfabrication process for the TPF DM. The added layer in step #6 combines two polysilicon deposition steps.

2.3. Device modeling

The nulling coronagraph specifications require all of the DM segments to have a deviation from flatness (i.e. flatness error) smaller than 10nm RMS. This segment flatness error budget encompasses segment bending during actuation as well as initial flatness errors due to fabrication. Residual stresses in the polysilicon fabrication process and print through from patterned layers below the mirror induce initial flatness errors. Segment bending occurs when the segment is tilted by differential actuation of the three surface-normal actuators. For pure piston motion, no segment bending is expected.

Bending is caused by moments that are imparted to the mirror segment through its posts connections. Either increasing the stiffness of the mirror segment or reducing these moments reduces mirror bending. Two mirror architectures were developed in parallel to test both of these concepts. The first architecture uses thick rigid mirror segments, and the second uses an actuator design that reduces bending moments imparted to the mirror by the actuator. In the new actuator design, flexure cuts are embedded in the actuator diaphragm surrounding the mirror's post attachment, which reduces the torsional stiffness of the actuator without significant loss in surface-normal stiffness. To design appropriate geometric dimensions for both the thick and the thin mirror architectures, both were modeled using a combination of finite element simulation (using CoventorWare and Intellisense MEMS modeling software) and first order mechanical approximations.

For the thick mirror architecture, the relationship between thickness of the epipoly (mirror) layer and segment bending during tilt actuation was estimated using a Coventor Ware finite element analysis. Mirror segment bending was analyzed over a range of segment thicknesses when the mirror was tilted to 3.5 mrad (Fig. 3). The results suggest that a total mirror segment thickness of 15 μm reduces mirror bending to less than 1 nm RMS. A total mirror segment thickness of 18 μm was selected

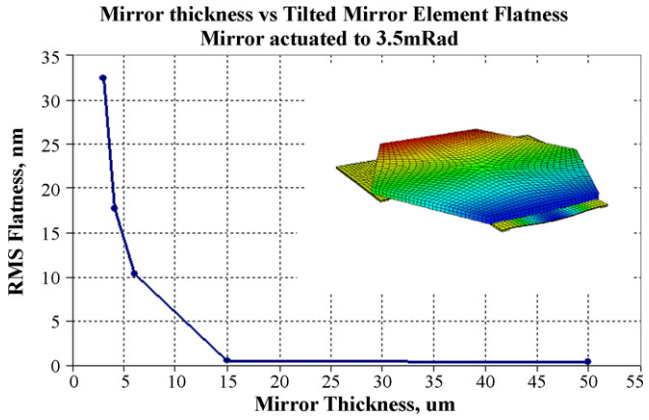

Fig. 3. RMS planarity after tilting. Mirror segment bending is plotted vs. epitaxial grown polysilicon thickness. Critical thickness for satisfying nulling coronagraph requirements is 15 μm.

for prototype fabrication. This corresponds to a 15 μm layer of epipoly and a 3 μm seed layer of polysilicon.

Alternatively, the second mirror design uses a thinner more compliant mirror segment layer, but employs flexures in the actuator diaphragm (Figs. 4 and 6) to reduce the magnitude of torsional loads imparted to the mirror segment by its posts when the segment is tilted. The flexure cuts are etched into the second polysilicon layer, encircling the post connection to the mirror segment, effectively providing a two-axis gimbal connection between the mirror and the actuator. To determine the mirror segment thickness and flexure dimensions for this mirror design, several first order approximations were combined with a finite element analysis.

The conventional actuator (without flexures) subjected to moment loading around a horizontal axis at the post is challenging to model analytically. As discussed above, the actuator diaphragm is comprised of a rectangular plate clamped along two parallel edges and free along the other two edges. Torsional rigidity for this structure depends on the orientation of the applied moment's axis. The device is more compliant to torsional moments applied around an axis parallel to the free edges than it is to moments applied around an axis parallel to the clamped edges. Neither case has a straightforward analyt-

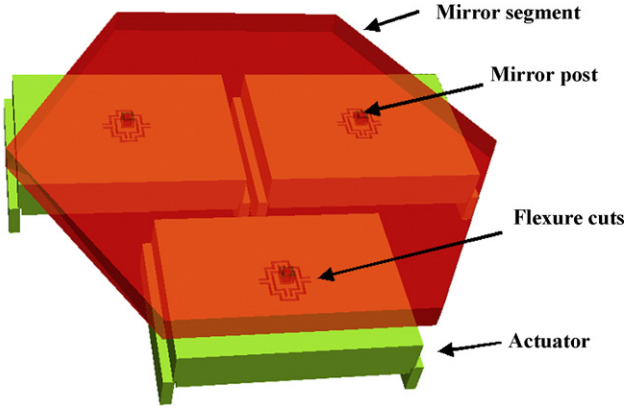

Fig. 4. 3D model of the flexure actuator design. The flexure cuts surround the mirror post, providing a 2-axis gimbal between the mirror and the actuator.

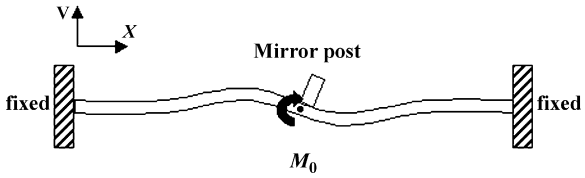

Fig. 5. Cross section of plate bending approximation for conventional actuator design.

ical solution. However, a first order approximation for which an exact analytical solution exists may be used to estimate the torsional rigidity of the conventional actuator along the stiffer axis (parallel to the clamped edges). In this approximation the plate is compared to a clamped–clamped beam subjected to a central moment M_0 at its center, as shown in Fig. 5. This is a reasonable approximation of an actuator loaded by a post spanning its width. Since the actual actuator post spans only 10% of the width, this model will over estimate the actual torsional stiffness of the actuator along this dimension.

As the mirror segment tilts, the actuator *beam* resists the applied moment M_0 with a torsional stiffness constant, k_c, equal to the ratio of the applied moment to the mirror tilt angle ϕ,

$$k_c = \frac{M_0}{\phi} \tag{1}$$

Assuming minimal surface-normal deflection, torsional stiffness can be determined by solving Euler's beam bending equation with the appropriate boundary conditions,

$$\frac{d^2V(x)}{dx^2} = \frac{-M(x)}{EI} \tag{2a}$$

$$V(0) = V(L_c) = 0 \tag{2b}$$

$$\left.\frac{dV}{dx}\right|_{x=0} = \left.\frac{dV}{dx}\right|_{x=L_c} = 0, \tag{2c}$$

where V is the actuator's displacement in the surface normal direction, E Young's modulus of elasticity (~160 GPa for polysilicon), I the beam's moment of inertia ($b_c t^3/12$, where b_c is the actuator width and t is the actuator thickness) and L_c is the actuator's span or length [7,8]. The gradient of the beam displacement V evaluated at the beam center, $L_c/2$, is equivalent to the mirror tilt angle ϕ,

$$\phi = \nabla V|_{x=L_c/2}. \tag{3}$$

Combining all terms and solving for the torsional stiffness of the actuator diaphragm we find,

$$k_c = \frac{4Eb_c t^3}{3L_c}. \tag{4}$$

When flexures are etched into the actuator diaphragm the mirror post dimensions approach those of the twisting body and the above approximation is no longer valid. A closer approximation to this mechanical system is to model the flexure arms as rectangular bars of polysilicon in torsion, as can be seen in Fig. 6.When the mirror segment tilts along a primary axis of the actuator, the torsional stiffness, k_f, for each flexure arm is determined using Eq. (1). The solution for a rectangular bar in

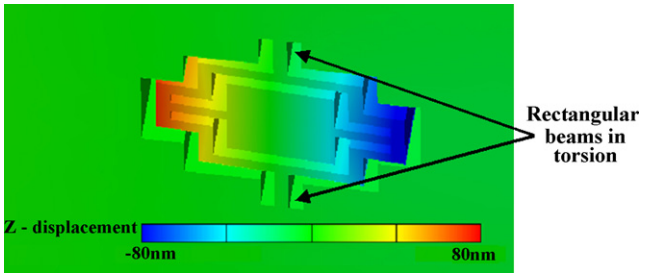

Fig. 6. Reverse side of actuator flexure post attachment as mirror segment is tilted. The flexures can be modeled as rectangular bars under torsion. The flexures reduce the torsional stiffness of the actuator post connection, which reduces bending moments imparted to the mirror segment during actuation.

torsion is well known (St. Venant's problem) and has a numerical solution [9]. Solving for the twist angle we find,

$$\phi = \frac{M_0 L_f}{\beta b_f t^3 G}, \tag{5}$$

where β is a solution parameter that depends on the width-to-thickness ratio, b_f/t, G the shear modulus ($E/2(1+\nu)$, where ν is Poisson's ratio, ~0.23 for polysilicon) and L_f is the length of the beam perpendicular to the twisting direction. The value of β corresponding to a width-to-thickness ratio of 1.5, typical for the flexure design, is approximately 0.196. The torsional stiffness of one flexure arm can then be determined by combining Eqs. (1) and (5), a factor of 2 is included to account for both flexure arms, leading to a total stiffness of,

$$k_f = \frac{2G\beta b_f t^3}{L_f}. \tag{6}$$

Comparing the two torsional stiffness constants for a conventional and flexure actuator of the same thickness, t, we find,

$$\frac{k_c}{k_f} = \frac{4(1+\nu)L_f b_c}{3\beta L_c b_f} = \frac{8.37 L_f b_c}{L_c b_f}. \tag{7}$$

Typical values for L_c and b_c are 265 and 200 μm, respectively. This corresponds to an estimated stiffness ratio of,

$$\frac{k_c}{k_f} = \frac{6.31 L_f}{b_f}. \tag{8}$$

Using a combination of Eq. (8) and finite element analysis, optimum dimensions for the flexure actuator design were determined. The value for b_f was selected to be the minimum feature size allowed in the fabrication process, 3 μm. The selection for L_f involved a tradeoff between reducing the actuator's torsional stiffness and maintaining its surface-normal stiffness. A large reduction in the surface normal stiffness changes device control properties and risks actuator failure, which is undesirable. By analyzing the mirror-bending results for a finite element model of a 3 μm thick mirror segment, a conservative value of 12 μm was selected for the flexure lengths. According to the analysis, flexures with these dimensions reduced mirror bending to less than 2 nm RMS at 3 mrad of mirror tilt, while reducing surface normal stiffness by approximately 15% (Fig. 7(a and b)). Mirror bending with conventional actuators is about 25 nm RMS at 3 mrad of tilt.

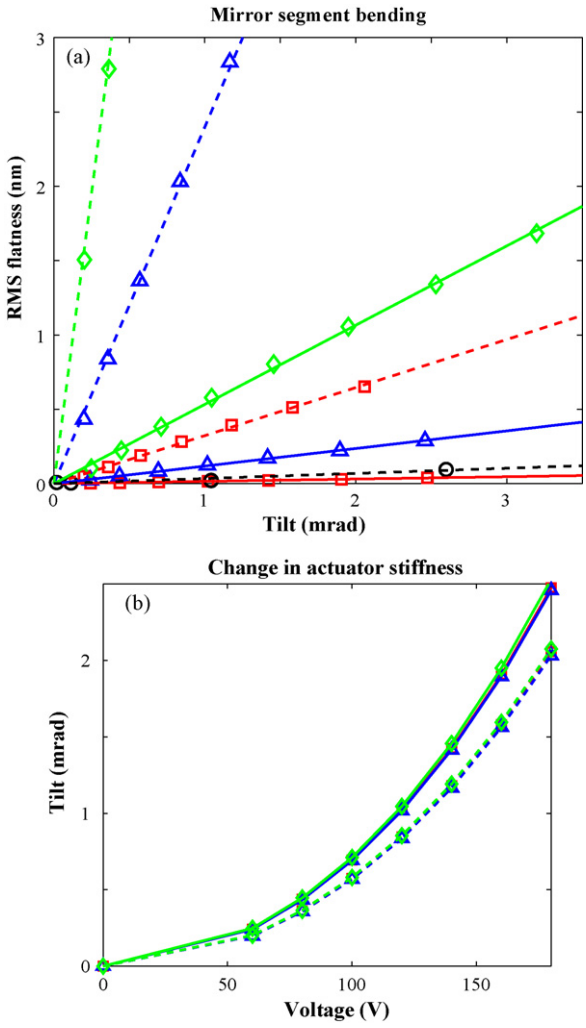

Fig. 7. Finite element simulation results. (a) RMS mirror segment bending (flatness) vs. mirror segment tilt. Flexure (solid line) and conventional (dashed line) actuator designs are compared for various mirror segment thicknesses (diamond: 3 μm, triangle: 5 μm, square: 10 μm, circle: 18 μm). For every voltage increment a cross section of the tilted mirror is measured and its RMS flatness calculated. A substantial reduction in mirror segment bending is achieved using the flexure cuts for a constant mirror segment thickness. A 3 μm thick mirror segment tilted to 3 mrad experiences less than 2 nm RMS of bending. (b) Mirror control voltage vs. mirror segment tilt. Flexure (solid) and conventional (dashed) actuator designs are compared for various mirror segment thicknesses. Greater tilt at lower control voltages implies reduced surface normal actuator stiffness. It is apparent that the mirror with flexure actuators tilts to higher angles at constant control voltages, implying a reduction in surface normal stiffness. <15% change at 2 mrad of tilt.

Plugging the above flexure width and length values into Eq. (8), we find the conventional actuator is approximately 25 times stiffer than the flexure actuator. To verify the validity of this approximation, a separate finite element simulation was performed in which an identical moment is applied at the center of each actuator design. Because the moment is identical, the ratio between torsional stiffness constants becomes the ratio of the flexure to conventional actuator twist angles,

$$\frac{k_c}{k_f} = \frac{\phi_f}{\phi_c}. \tag{9}$$

Measurements of these twist angles from the simulation results suggest that the conventional actuator is 20–30 times stiffer than the flexure actuator (depending on the axis of the applied moment), verifying our beam approximation.

For ease in prototype manufacturing, the mirror segment thickness for the thin mirror architecture was selected to be the thickness of the seed layer used for the thick epipoly mirror architecture, 3 μm. As will be discussed below, by reducing the mirror segment thickness, mirror curvature due to residual stresses becomes more manageable. A thick mirror segment that is curved due to residual stresses is more difficult to flatten via post-processing than a thinner mirror.

3. Device characterization

3.1. Electromechanical performance

The first prototype devices for the new TPF DM consisted of several arrays with 18 and 3 μm thick mirror segments (with and without the epipoly layer) using conventional and flexure electrostatic actuators. The electromechanical performance and optical quality of these prototype arrays were measured using interferometric surface mapping microscopes. To test the electromechanical behavior of a TPF DM segment, a single mirror segment actuator was energized at a time, tilting the mirror along one of its three primary axes. The net motion of the mirror segment is determined by taking the difference between two topography measurements, before and after the segment is tilted. This results in a direct calculation of mirror bending during actuation. To a first order, the difference measurement loses information regarding the initial mirror shape.

Preliminary characterization of mirror segment tip/tilt behavior on the three primary axes was performed using a Wyko NT2000 optical profiler in VSI mode. With the microscope CCD at half resolution, the average noise floor for the instrument was determined to be 6.6 ± 0.9 nm RMS, largely due to high frequency laboratory vibrations that move the sample small lateral amounts between measurements. This value was determined through successive difference measurements of a mirror that was not actuated. The reduction in CCD resolution (increasing the CCD pixel bin size) is similar to applying an averaging filter to the data. Difference measurement data was processed using a Matlab routine that extracted and fit the tilted mirror data to a plane, from which RMS flatness and mirror tilt were calculated. Mirror tilt and bending results for seven 3 μm thick mirror segments with conventional or flexure actuators can be seen in Fig. 8.

The noise floor for the instrument has been subtracted (in quadrature) from the mirror bending data. Therefore a value of zero corresponds to a measurement that is less than or equal to the noise floor. It is apparent from the data that other noise terms exist which affect instrument accuracy. One of these is assumed to be the initial mirror shape, which is not completely removed in the difference measurement. As discussed below, the mirrors tend to be cup shaped due to the stress gradients in the polysilicon mirror layer. Nevertheless, these results suggest

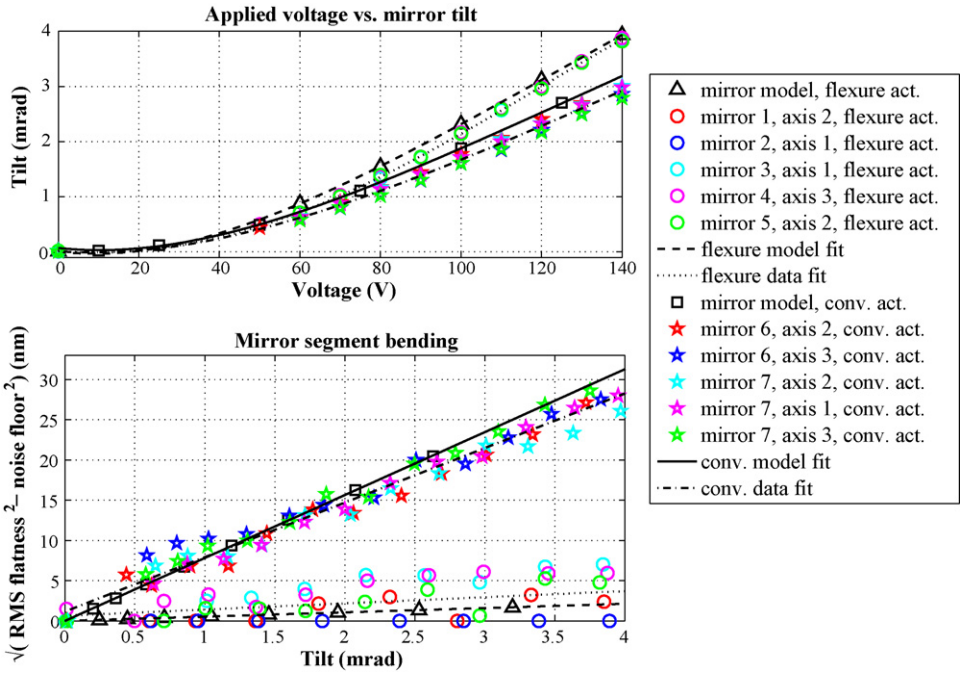

Fig. 8. Wyko characterization of TPF DM segments that are 3 μm thick and controlled using the conventional or flexure actuator design. Control voltage vs. tilt (top) and mirror segment bending vs. tilt (bottom). Mirror segment bending for the flexure actuator is close to the instrument noise floor. At 3 mrad of tilt, bending is 3 nm RMS above noise floor.

that a 3 μm thick mirror using flexure actuators experiences less than 10 nm RMS of bending during actuation.

To obtain a more accurate picture of mirror segment bending for the 3 μm thick mirror with flexure actuators, a Zygo NewView 6000 optical profiling microscope was used with a noise floor of 4.1 Å RMS. Unfortunately the instrument was used in a trial run and only a few measurements were recorded at the time of this publication. The difference measurement results for a mirror tilted to 4.3 mrad with the best-fit plane term removed can be seen in Fig. 9. The planarity (bending) of the mirror segment at 1.3 mrad of tilt was found to be 1.14 nm RMS and at 4.3 mrad of tilt, 2.83 nm RMS. This is in agreement with the simulation results shown in Figs. 7(a) and 8, which found the mirror bending to be 1.02 nm RMS at 1.3 mrad of tilt and 2.78 nm RMS at 4.3 mrad of tilt.

The electromechanical characterization for the thick mirror design (with conventional actuators) is shown in Fig. 10. By increasing the thickness of the mirror segment to 18 μm (using the epitaxial polysilicon growth process discussed above), mirror segment bending is also reduced to the noise level of the Wyko NT2000 interference microscope. With the microscope CCD at quarter resolution, the average noise floor for the Wyko instrument was reduced to 5.2 ± 0.6 nm RMS for these difference measurements. The results suggest that an 18 μm thick mirror using conventional actuators also experiences less than 10 nm RMS of bending during actuation. This is in agreement with the finite element simulation performed for the thick mirror design (Fig. 3).

Although the results presented thus far consist of mirror tilting without simultaneous piston motion, no change in mir-

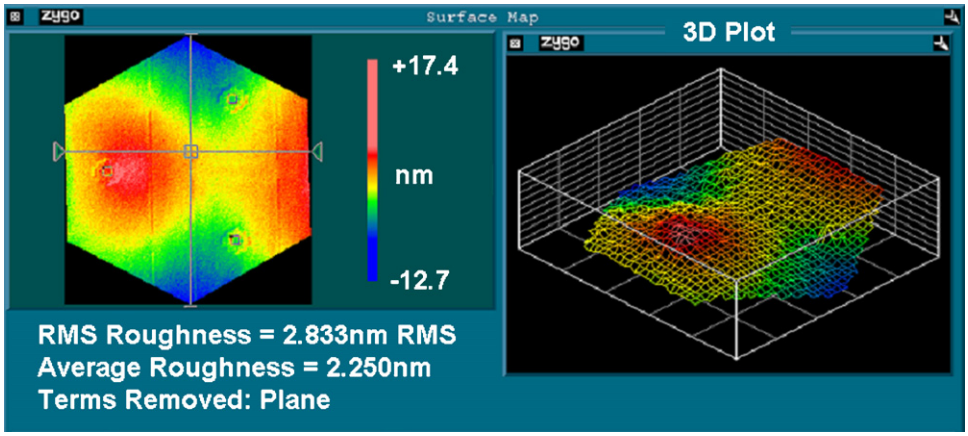

Fig. 9. Zygo NewView difference measurement of a 3 μm thick TPF DM segment with flexure actuators tilted to 4.3 mrad. The mirror bending, seen in the surface maps on both the left and right, was found to be 2.83 nm RMS.

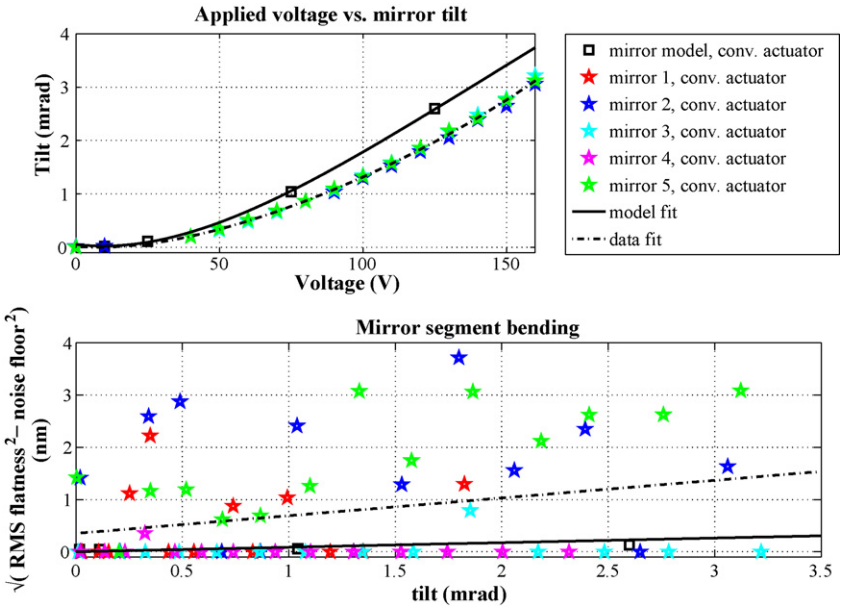

Fig. 10. Wyko characterization of TPF DM segments that are 18 μm thick and controlled using the conventional actuator design. According to the results (which are near the instrument noise floor), mirror segment bending is 1.5 nm RMS above noise floor at 3 mrad of tilt. Control voltage vs. tilt (top) and mirror segment bending vs. tilt (bottom).

ror bending behavior was observed when simultaneous piston motion was examined. Also apparent in the voltage versus tilt data of Figs. 8 and 10 is a slight shift between simulation and experimental data curves. The experimental results are shifted towards higher operating voltages than their corresponding finite element simulations because the fabricated actuator diaphragms are actually stiffer than their model counterparts. Actuator stiffness is dependent on the average in-plane biaxial stress of the diaphragm polysilicon layer. These stresses are estimated by the foundry and used in the models. The offset is a result of error in this estimation.

3.2. Optical quality

The nulling coronagraph requires each DM segment to have a surface flatness of less than 10 nm RMS. This error budget includes the segment's initial shape and any bending it experiences during tip/tilt actuation. A larger reduction in mirror bending provides more leeway for the mirror's initial shape, which is the impetus behind the work described above. If mirror bending is limited to 3 nm RMS, the mirror's initial shape must have flatness better than 9.5 nm RMS to satisfy these requirements. A mirror segment's initial shape is dominated primarily by the residual stress gradient in the deposited or grown polysilicon mirror layer, which is a very difficult quantity to control. The sign of the average stress gradient determines if the segments curl up or down. The mirror's optical quality can also be affected by print through of micromachined layers below the mirror layer. Neglecting all disfigurement terms except for curvature, a 9.5 nm RMS flatness corresponds to a radius of curvature of approximately 1.15 m for each mirror segment.

In terms of optical quality, the main difference between the thick and the thin mirror segment designs is the use of the epipoly layer in the thick design. The optical quality for mirrors fabricated using both designs was measured using the Wyko NT2000. Typical surface quality for both architectures can be seen in

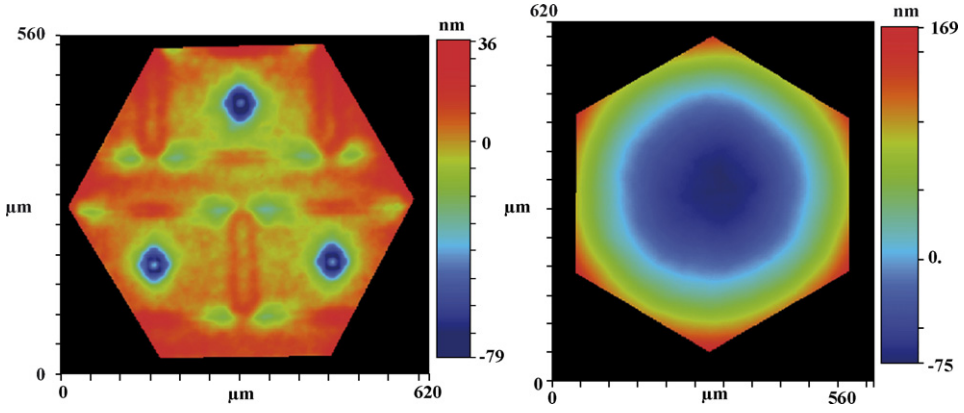

Fig. 11. Typical mirror optical quality measured using Wyko NT2000. The thin mirror design (left) has a radius of curvature of 1.7 m (14.1 nm RMS flatness). The thick mirror design (right) has a radius of curvature of 170 mm (55.3 nm RMS flatness).

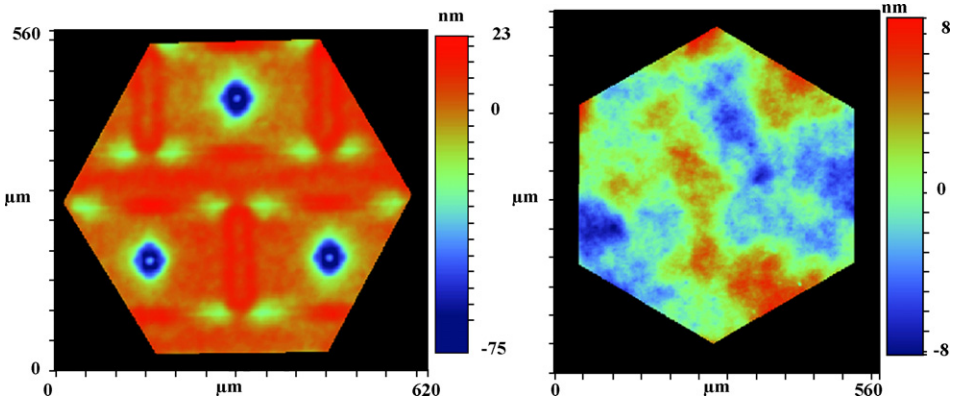

Fig. 12. Curvature terms are removed from the measurements in Fig. 11 to examine polishing and print-through results. The surface flatness measured for these mirror segments is 12.6 nm RMS (left) and 2.8 nm RMS (right), for the thin and thick mirror architectures, respectively.

Fig. 11. DM segments fabricated with the thick mirror architecture are cup shaped due to significant stress gradients in the epipoly mirror layer. Their average radius of curvature is about 151 ± 7 mm. This mirror shape was very uniform across all of the DM segments in several smaller 61-element test arrays. Devices fabricated using flexure actuators and the thin mirror architecture have an average radius of curvature of 1.5 ± 0.25 m. This curvature is also due to stress gradients in the thin mirror layer, but because the layer is thinner, its curvature can be manipulated using a variety of techniques discussed below.

To gain a better understanding of local surface roughness for the two mirror designs, the curvature terms can be removed from the datasets in Fig. 11. These results are displayed in Fig. 12. The thick mirror process produced an average surface roughness of 2 nm RMS, which is near the noise floor of the Wyko NT2000 operating in PSI mode. According to measurements performed by the polishing vendor, this local surface roughness is below 1nm RMS. Alternatively, the thin mirror design has an average surface roughness of about 13nm RMS, largely due to print-through. A significant advantage of the thick mirror design is its ability to rid the mirror segment surface of this print-through.

4. Discussion

Although neither of the TPF DM designs presented here satisfies the 10 nm RMS flatness requirement for the nulling coronagraph, a hybrid using aspects of both designs is proposed. While the thin mirror architecture satisfies the curvature requirement necessary for the coronagraph, it misses because of its local roughness caused by print-through. Conversely, the thick mirror architecture has the local surface roughness needed by the coronagraph, but has too much curvature induced by embedded stress gradients. It is also too thick for curvature manipulation. A hybrid device that uses a thin (0.5 μm) seed layer for growing a thick (10 μm) epipoly mirror layer is proposed. The thick epipoly layer can be polished to a thinner (5–8 μm) mirror segment that will be free of print-through, capable of curvature post-processing, and rigid enough to resist bending moments if flexure actuators are used.

The most significant task remaining for the successful fabrication of the TPF DM is the development of a method to correct mirror curvature. Several methods exist to change stress gradients embedded in thin polysilicon films, such as high temperature furnace anneals to relax the gradient [10], combined with impurity doping to counteract residual stresses [11]. A significant research effort is currently underway at BU to explore how annealing and doping can affect the stress gradients in the epipoly mirror layer, which has a slightly different polycrystalline grain structure than the conventional CVD polysilicon layer (that of the actuator layer).

An alternative method developed at BU to flatten released mirrors requires stress gradients that curl the mirror upwards. The process uses the implantation of inert gases in the mirror surface to create a thin layer of compressively stressed material that acts to flatten the mirror segment [12]. The physical premise is similar to that used by doping methods for counteracting stress gradients. Lastly, the deposition of thin metal films with either compressive or tensile stress properties for the mirror's reflective layer (chromium and gold) can also be used to counteract the average stress gradient (described by Stony's equation [11]). Research efforts exploring the feasibility of this curvature "tuning" mechanism is also underway.

5. Conclusion

Realization of the TPF DM for the nulling coronagraph will set new milestones for MEMS DMs in optical quality and micromirror control. If successfully implemented, this DM will also become one of the first MEMS-based DMs used in a space-based astronomical observatory. DM development has overcome several technological challenges, such as a new fabrication layout to accommodate hexagonal mirror segments with ±3 mrad of out-of-plane rotation (tilt) and 1 μm of surface normal motion (piston), simultaneously. Furthermore, two new mechanical designs have been developed that prevent mirror bending during motion. The first design uses a 15 μm thick epitaxial grown polysilicon layer to add structural rigidity to the DM segment, reducing bending to less than 10 nm RMS, while greatly improving mirror-polishing results to create optical surfaces with less than 2 nm RMS local surface roughness. The second design uses a thinner 3 μm thick mirror design with new flexure actuators that reduce bending moments imparted to the

mirror segment. The use of flexures reduces mirror bending to less than 3 nm RMS at 4.3 mrad of tilt, and although the optical quality of the mirror surface suffers from print-through, its reduced thickness is easier to manipulate via post-processing. A variety of curvature processing techniques have been proposed and are currently being researched. A future hybrid DM that combines the benefits of both designs is proposed to satisfy the nulling coronagraph λ/100 optical and electromechanical control requirements.

Acknowledgements

Thanks to Farhaan Razi for his help with the electromechanical characterization of the mirror segments. This work was supported by a NASA/JPL award number 1254441.

References

[1] Terrestrial Planet Finder Web Page: http://planetquest.jpl.nasa.gov/TPF/tpf_index.cfm, 2007.
[2] B.M. Levine, M. Shao, D. Liu, J.K. Wallace, B. Lane, Planet detection in visible light with a single aperture telescope and nulling coronagraph, Proc. SPIE 5170 (2003) 200–208.
[3] B.M. Levine, M. Shao, C.A. Beichman, B. Mennesson, R. Morgan, G. Orton, E. Serabyn, S. Unwin, T. Velusamy, N. Woolf, Visible light terrestrial planet finder—planet detection and spectroscopy by nulling interferometry with a single aperture telescope, Proc. SPIE 4852 (2003) 221–229.
[4] J.B. Stewart, T.G. Bifano, P. Bierden, S. Cornelissen, T. Cook, B.M. Levine, Design and development of a 329-segment tip–tilt–piston mirror array for space-based adaptive optics, Proc. SPIE 5894 (2005).
[5] T.G. Bifano, J. Perreault, R.K. Mali, M.N. Horenstein, Microelectromechanical deformable mirrors, J. Select. Top. Quant. Electron. 5 (1999) 83–90.
[6] T.G. Bifano, R. Mali, J. Perreault, K. Dorton, N. Vandelli, M. Horentein, D. Castanon, Continuous membrane, surface micromachined silicon deformable mirror, Opt. Eng. 36 (5) (1997) 1354–1360.
[7] R.J. Roark, W.C. Young, Formulas for Stress and Strain, McGraw-Hill, New York, 1982.
[8] S. Timoshenko, S. Woinowsky-Krieger, Theory of Plates and Shells, McGraw-Hill, New York, 1987.
[9] E. Popov, Engineering Mechanics of Solids, Prentice Hall, New Jersey, 1999.
[10] X. Zhang, T. Zhang, M. Wong, Y. Zohar, Rapid thermal annealing of polysilicon thin films, J. Microelectromech. Syst. 7 (1998) 356–364.
[11] M. Madou, Fundamentals of Microfabrication, CRC Press, New York, 2002.
[12] T.G. Bifano, H.T. Johnson, P. Bierden, R.K. Mali, Elimination of stress induced curvature in thin-film structures, J. Microelectromech. Syst. 11 (2002) 592.

Biographies

Jason B. Stewart is a PhD candidate in the Department of Electrical and Computer Engineering at Boston University. He received his BA degree from Colgate University in Physics in 2000, and his MS degree from Boston University in Electrical Engineering in 2004. He is presently a research assistant for Professor Thomas Bifano in the Precision Engineering Research Laboratory. His current research is focused on the fabrication and control of MEMS deformable mirrors for high-resolution wavefront control in space-based astronomical observatories. His other research interests include adaptive optics and semiconductor optoelectronic devices.

Thomas G. Bifano received his BS and MS degrees in Mechanical Engineering and Materials Science from Duke University in 1980 and 1983, respectively, and a PhD in Mechanical Engineering from North Carolina State University in 1988. He is currently the Director of the Boston University Photonics Center, Professor of the Department of Manufacturing Engineering and the Chief Technical Officer of Boston Micromachines Corporation. Since joining the faculty of Boston University in 1988, he has developed an internationally known research program to study ultraprecision machining. He directs the Boston University Precision Engineering Research Laboratory, where he studies sensing, control, and fabrication at the limits of achievable precision. Areas of research interest include microelectromechanical systems (MEMS), nanometer-scale actuation, micromachining, design of optical arrays, and microfluidics.